NANO LETTERS

Letter

pubs.acs.org/NanoLett

Direct Imaging of Free Carrier and Trap Carrier Motion in Silicon Nanowires by Spatially-Separated Femtosecond Pump–Probe Microscopy

Michelle M. Gabriel, Justin R. Kirschbrown, Joseph D. Christesen, Christopher W. Pinion, David F. Zigler, Erik M. Grumstrup, Brian P. Mehl, Emma E. M. Cating, James F. Cahoon,* and John M. Papanikolas*

Department of Chemistry, University of North Carolina at Chapel Hill, Chapel Hill, North Carolina 27599-3290, United States

ABSTRACT: We have developed a pump–probe microscope capable of exciting a single semiconductor nanostructure in one location and probing it in another with both high spatial and temporal resolution. Experiments performed on Si nanowires enable a direct visualization of the charge cloud produced by photoexcitation at a localized spot as it spreads along the nanowire axis. The time-resolved images show clear evidence of rapid diffusional spreading and recombination of the free carriers, which is consistent with ambipolar diffusion and a surface recombination velocity of ~10^4 cm/s. The free carrier dynamics are followed by trap carrier migration on slower time scales.

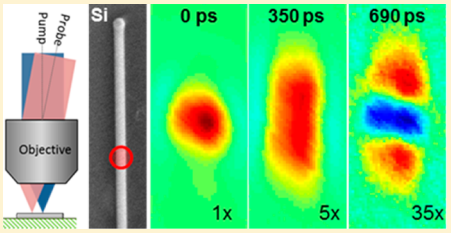

KEYWORDS: *Ultrafast microscopy, silicon nanowire, carrier diffusion, pump–probe spectroscopy*

The motion of charge carriers through nanoscale structures is of central importance to many emerging technologies in nanoscale electronics, optoelectronics, and solar energy conversion.[1−4] The interaction of charge carriers with the surfaces, localized defects, and electrical contacts in nanostructured devices can have a profound influence on the migration of electrons and holes through a semiconductor structure. These effects have generally been inferred through optical and electrical measurements that average over an entire structure, or an ensemble of structures, and do not directly measure the local carrier motion. To acquire this information, methods with submicrometer spatial resolution and picosecond temporal resolution are needed. The pursuit of such methods is not new, and time-resolved optical microscopies have been applied to a broad range of problems.[5−18] The most common approaches are emission-based but are limited to the picosecond time range and require fluorescent samples. Pump–probe methods provide access to faster time scales but are more difficult to implement. Nevertheless, several recent reports from our group,[5,6] and others,[10−18] describe their extension to microscopy, particularly in far-field configurations.

Here, direct imaging of carrier motion in Si nanowires is accomplished using a pump–probe microscope that can excite a structure in one location and monitor the arrival of photoexcited carriers in another. Similar examples[19−22] have appeared in the literature. In this work, we present results with diffraction-limited pump–probe beams that provide a high (submicrometer) lateral resolution. This unique configuration permits the collection of spatially separated pump–probe (SSPP) *images*, allowing direct visualization of the carrier population over time. This capability permits us to distinguish between rapid free carrier motion and the slower migration of trapped carriers, as discussed below.

Intrinsic Si nanowires (i-Si) were grown by a vapor–liquid–solid (VLS) mechanism[23] using a home-built, hot-wall chemical vapor deposition (CVD) system.[3] For a typical growth run, Au nanoparticles with diameters of ~250 nm were dispersed on Si (100) wafers coated with 600 nm thermal oxide, and these wafers were inserted into the center of a quartz-tube furnace. Nanowires were grown with a total reactor pressure of 40 Torr using a gas flow of 2.00 standard cubic centimeters per minute (sccm) silane and 200 sccm hydrogen as carrier gas. The reactor was held at 600 °C for 2 min to nucleate wire growth and then cooled (10 °C/min) to 450 °C for continued wire growth over two hours. For n-type Si nanowires (n-Si), an additional flow of 10.00 sccm phosphine (1000 ppm in hydrogen) was used to provide a source of phosphorus dopant at a relative concentration of ~200:1 Si:P. After completion of wire growth, nanowires were thermally oxidized at 1000 °C for 60 s in 100 Torr flowing oxygen to form a 5–10 nm-thick thermal oxide. Nanowires were then mechanically transferred onto quartz substrates for microscopy imaging.

The transient absorption microscope is illustrated in Figure 1. The 850 nm output of a mode-locked Ti:Sapphire oscillator is split by a 10/90 beam splitter. The higher power beam is frequency doubled to 425 nm and used as the pump, while the other is used as the probe. Two synchronized acousto-optic modulator (AOM) pulse pickers reduce the repetition rates of the pump and probe beams to 1.6 MHz, thus ensuring complete relaxation before the next pump–probe pulse pair arrives at the sample. A motorized linear stage controls the time delay between excitation and probe pulses. Both the pump and probe beams are attenuated to 20 pJ per pulse, recombined

Received: January 21, 2013
Published: February 19, 2013

   dx.doi.org/10.1021/nl400265b | *Nano Lett.* 2013, 13, 1336–1340

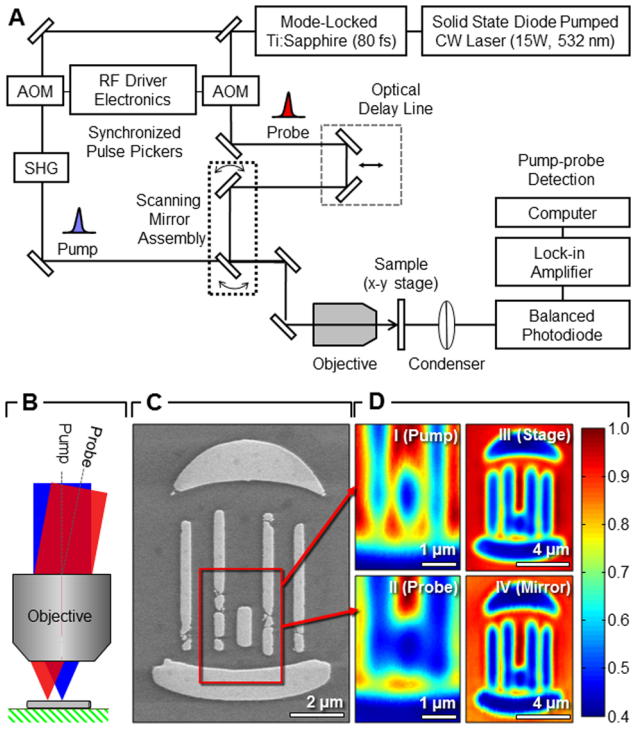

Figure 1. Overview of the experimental system. (A) Illustration of the spatially separated pump−probe (SSPP) microscope. An x−y scanning stage positions the structure under the 425 nm pump spot; the 850 nm probe spot is positioned relative to the pump with a scanning mirror assembly. (B) Schematic illustration of spatially separated scanning. (C) SEM image of the UNC logo defined in Au by electron-beam lithography; scale bar, 2 μm. (D) Left, optical transmission images obtained with the pump (I) and probe (II) beams scanned over a lower-center portion of the Au structure, as denoted by the inset box in panel C, that contains an ∼400 nm gap; scale bars, 1 μm. Red indicates maximum transmission and blue minimum transmission. Right, comparison of transmission images acquired by raster-scanning the probe beam over the entire Au structure shown in panel C using either the x−y stage (III) or the mirror assembly (IV); scale bars, 4 μm.

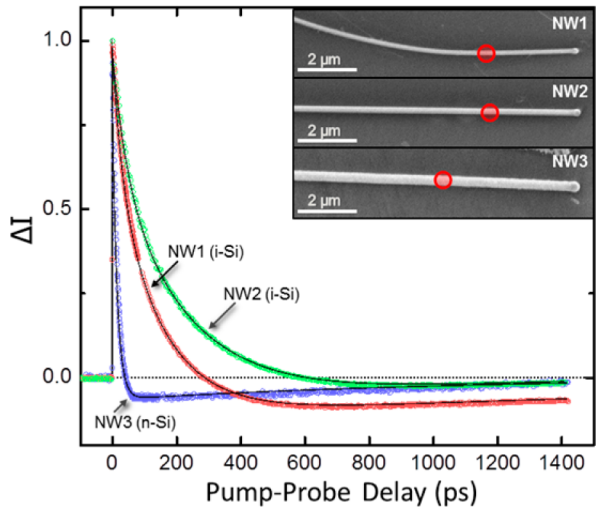

Figure 2. Normalized pump−probe microscopy decay kinetics following photoexcitation of a localized region in three different Si nanowires; NW1 (red) and NW2 (green) are intrinsic, and NW3 (blue) is n-type. All three were fit to a triexponential decay (solid lines, see Table 1 for fitting parameters). Inset: SEM images of the three wires showing the location of pump excitation as a red circle; scale bars, 2 μm.

using a dichroic beam splitter, and then directed onto the back aperture of a 50× (0.8 NA) objective that focuses them to diffraction limited spots within a single structure. Diffraction limited spatial resolution in our instrument has been confirmed in two-photon emission images.[5] Images of the UNC logo defined in Au on a quartz substrate (Figure 1C) obtained using the pump and probe beams (Figure 1D) are consistent with diffraction-limited focusing of the two spots, with the pump spot being smaller than the probe. The probe beam is collected by a condenser lens, filtered to remove residual pump light, and directed onto a balanced photodiode. The pump beam is modulated at 10 kHz using the AOM, and pump-induced changes in the intensity of the probe pulse are monitored by a digital lock-in amplifier, producing the measured change in intensity, ΔI, plotted in the figures discussed below. The time-resolution of the instrument is ∼500 fs.[5,6]

Initial experiments were performed by measuring kinetics from spatially overlapped pump and probe beams positioned 3−5 μm from the end of three nanowire samples (Figure 2). We estimate that photoexcitation by the pump pulse produced $\sim 10^{19}$−10^{20} carriers/cm^3 assuming an absorption efficiency of 10−100% at the excitation wavelength of 425 nm.[1,2] Pump−probe transient signals are shown for two i-Si wires, NW1 and NW2, and an n-Si wire, NW3, with diameters of 160, 210, and 330 nm, respectively. Exact locations of excitation are indicated on the respective SEM images in Figure 2. The two i-Si NW transient signals exhibit an intense positive going (bleach) feature that becomes weakly negative (absorptive) at several hundred ps before returning to zero signal. These transient signals are similar to pump−probe measurements performed on ensembles of Si nanowires.[24] The signals include contributions from the free carrier (electron and hole) and trap carrier populations and can arise from changes in absorptivity and/or reflectivity upon photoexcitation as well as carrier lensing effects due to the spatially localized excitation.[5,6]

All three transient signals can be well fit to a superposition of a positive going signal that decays with biexponential kinetics (τ_1, τ_2), and a smaller negative going signal with a much slower decay time, τ_3 (see Table 1).[25] The two i-Si wires exhibit different decay kinetics, with NW1 showing a faster initial decay (τ_{avg} = 67 ps) than NW2 (τ_{avg} = 112 ps), but with a slower recovery time back to zero signal, τ_3 = 2300 ps (NW1) versus 551 ps (NW2). We attribute the initial decay to free carrier recombination and diffusion and the slower, negative amplitude component to trapped carrier recombination. For semiconductor nanowires, surface recombination is often the predominant recombination mechanism, and the surface recombination velocity, S, can be calculated from the carrier lifetime, τ, as $S = d/4\tau$, where d is the nanowire diameter.[3,4,26,27] The values derived from this analysis using the measured τ_{avg} are 6.0 × 10^4 cm/s and 4.7 × 10^4 cm/s for NW1 and NW2, respectively. These values are upper limits to the actual surface recombination velocities because Auger recombination and carrier diffusion (discussed below) also contribute to the decay. Nevertheless, the similarity between the S values for these two wires suggests that the initial decay is dominated by a surface recombination mechanism.

The n-Si wire (NW3) shows a much faster initial decay (τ_{avg} = 11 ps) and recovers with τ_3 = 1146 ps. The origin of the much faster decay in the n-Si wire is possibly a result of

dx.doi.org/10.1021/nl400265b | Nano Lett. 2013, 13, 1336−1340

Table 1. Parameters Used To Fit Kinetics Derived from Pump−Probe Microscopy to a Sum of Three Exponentials, $\Delta I(t) = A_1 e^{-t/\tau 1} + A_2 e^{-t/\tau 2} + A_3 e^{-t/\tau 3}$

	τ_1 (A_1)		τ_2 (A_2)		τ_3 (A_3)		τ_{avg} [a]
NW1	29.8 ps	(0.34)	144 ps	(0.78)	2300 ps	(−0.12)	67 ps
NW2	46.8 ps	(0.34)	248 ps	(0.87)	551 ps	(−0.23)	112 ps
NW3	1.75 ps	(0.06)	15 ps	(1.01)	1146 ps	(−0.07)	11 ps

[a]Average decay time for the two fast components, i.e., $(1/\tau_{Avg}) = [(A_1/\tau_1) + (A_2/\tau_2)]/(A_1 + A_2)$.

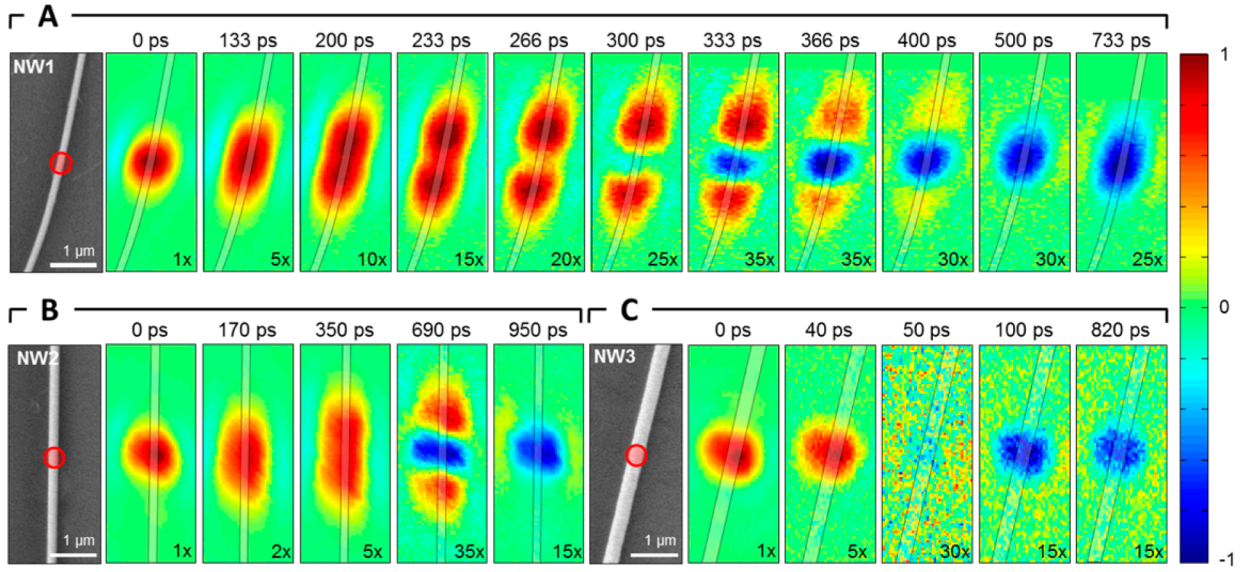

Figure 3. Time-resolved SSPP microscopy images. (A) NW1, (B) NW2, and (C) NW3. Left, SEM images of 5 μm sections of each wire centered around the pump laser excitation spot; (image sizes, 2 μm × 5 μm; scale bars, 1 μm). The location of the excitation spot is depicted by the red circle. For each sample, the tip of the wire lies beyond the top of the image. Right, series of SSPP images acquired at the pump−probe delay times denoted above each image. Location of the nanowire is depicted by the faint lines. Each image is 2 μm × 5 μm and is depicted using a normalized color scale with the relative amplitudes indicated by the scaling factors in the bottom-right corner of each image.

increased Auger recombination due to the high electron majority-carrier concentration. A second possibility is the presence of an amorphous Si shell surrounding the crystalline core, as suggested by the rougher surface and larger diameter observed in the SEM image. Regardless of the exact origin, the electron−hole recombination rate in this n-Si wire is substantially greater than the i-Si wires.

To characterize the diffusion process in the Si nanowires, we have directly imaged charge carrier motion using SSPP microscopy, in which the structure is excited in one location and probed in another. This experiment is accomplished by incorporating two separate positioning mechanisms for the pump and probe beams. The pump spot is positioned over a particular point in the structure through adjustment of the x−y sample stage. Independent placement of the probe beam is accomplished by directing it through a pair of mirrors with computer-controlled actuators, which vary the angle of the probe beam relative to the fixed pump beam (Figure 1A). The use of two (master/slave) mirrors allows adjustment of this angle while keeping the beam centered on the objective aperture. By scanning this angle, the position of the focused probe spot can be displaced from the pump by a distance (Δ_{pp}) of 10−20 μm while still remaining within the objective's field of view. Figure 1D compares transmission images taken using the scanning mirror assembly and the scanning stage. Both transmission images reproduce not only the general shape, but also the finer details of the structure, and the similarity of these two images to the SEM image demonstrates the distortion-free imaging capability of this scanning mechanism.

The SSPP microscope can be operated in two different modes. In one operational mode, the delay time between the pump and probe beams is held fixed, and the spatial displacement of the pump and probe is scanned, resulting in an image of the spatial variation in the transient absorption signal at a particular time after photoexcitation. SSPP images are shown for three different nanowires (NW1, NW2, and NW3) in Figure 3. At early pump−probe delays (near Δt = 0 ps), the images show an intense positive (red) transient absorption feature, with a spatial extent commensurate with the size of the pump spot. For the i-Si wires (NW1 and NW2), this spot spreads rapidly along the long axis of the nanowire, growing 4−5 μm in length during the first 300−500 ps. At the pump−probe delay time in which the transient signal crosses zero (refer to Figure 2), a trough appears at the location of the excitation spot that eventually becomes a net negative signal. The final images show the positive features disappearing altogether, leaving behind a negative (blue) region that broadens on a slow time scale. We attribute the rapid evolution of the intense positive signal to the diffusion of free carriers (electrons and holes) out of the excitation volume and the negative signal at long times to trap carrier motion. Rapid electron−hole recombination in the n-Si wire (NW3), on the other hand, limits the extent of spatial diffusion, and the initial feature shows no substantial broadening.

dx.doi.org/10.1021/nl400265b | Nano Lett. 2013, 13, 1336−1340

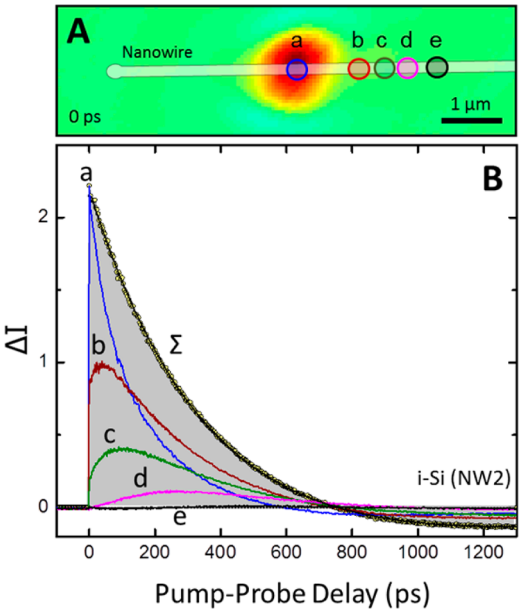

Figure 4. Spatially separated pump–probe (SSPP) transient signals. (A) SSPP image obtained at $\Delta t = 0$ overlaid with the spatial locations, a–e, of the displaced probe beam, which correspond to separations of $\Delta_{pp} = 0$, 1.02, 1.45, 1.83, and 2.32 μm, respectively; scale bar, 1 μm. (B) Transient signals obtained from NW2 by fixing the spatial separation, Δ_{pp}, between the pump and probe spots and scanning the pump–probe delay. The curves labeled a–e correspond to the positions indicated in panel A. Also shown is the transient signal, labeled $\sum$, obtained by summation of the individual SSPP signals. Individual data points are denoted by open yellow circles, and the solid line is a fit to $\Delta I(t) = A_1 e^{-t/\tau 1} + A_2 e^{-t/\tau 2}$ with $\tau_1 = 380$ ps ($A_1 = 3.21$) and $\tau_2 = 900$ ps ($A_2 = -1.02$).

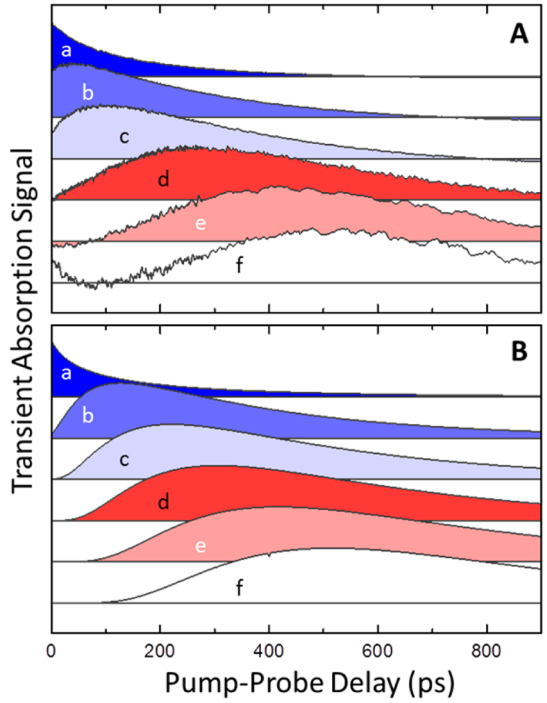

Figure 5. Experimental and simulated transient signals. (A) Normalized SSPP transient signals obtained from NW2. The curves labeled a–f correspond to separations $\Delta_{pp} = 0$, 1.02, 1.45, 1.83, 2.32, and 2.76 μm, respectively. (B) Analogous set of SSPP curves predicted by eq 1 using $D = 18$ cm^2/s and $\tau = 380$ ps. The pump and probe laser profiles have full width at half maximum values of 350 and 700 nm, respectively, and are included in the simulation curves.

The second operational mode of the SSPP microscope fixes the displacement between the pump and probe laser spots and scans the delay time between them. Figure 4 shows decay traces for five different separations, Δ_{pp}, along the NW2 nanowire axis. When the pump and probe are spatially coincident ($\Delta_{pp} = 0$), the maximum signal intensity is observed at $\Delta t = 0$ ps. A delayed rise in the signal is observed when the probe pulse is positioned away from the excitation spot ($\Delta_{pp} > 0$), reflecting the time needed for carriers to migrate from the pump region to the probe region. There is also an overall decrease in the intensity of the signal as the pump–probe separation is increased. At $\Delta_{pp} = 2.32$ μm, the overall intensity of the signal makes it difficult to discern the arrival of carriers when depicted on an absolute scale (Figure 4); however, when the transients are displayed normalized to their respective maxima (Figure 5A), it is clear that free carriers are migrating as far as 2.7 μm from the excitation region. These time-resolved data indicate that the spatially coincident pump–probe transient signals shown in Figure 2 are influenced by the diffusional motion of charge carriers away from the excitation region. In principal, the summation of transient signals obtained at different pump–probe separations (shown as the curve $\sum$ in Figure 4) should reflect the total free carrier population and remove effects from diffusional motion. This curve is well fit to a superposition of decays with positive and negative amplitudes; however, unlike the $\Delta_{pp} = 0$ μm signal, the decay of the positive signal in the superposition is reproduced by a single exponential with time constant of $\tau = 380$ ps, providing a more accurate measure of the free carrier lifetime. This value for τ gives a revised surface recombination velocity for NW2 of 1.4×10^4 cm/s, which is comparable to the value, $S = 7 \times 10^3$ cm/s, determined for wires grown under similar growth conditions.[3]

To quantitatively interpret the charge carrier motion observed with SSPP microscopy, we have developed a simple model that includes ambipolar diffusion of the free carrier population, a recombination process with a single first-order rate constant ($1/\tau$), and Gaussian profiles that represent the pump and probe laser beams centered at $x = 0$ and $x = \Delta_{pp}$, respectively. In this model, the number of carriers interacting with the displaced probe beam can be written as:

$$N(\Delta_{pp}, t) = \int_{-\infty}^{\infty} I(x - \Delta_{pp})\eta(x, t)\mathrm{d}x \quad (1)$$

where $I(x - \Delta_{pp})$ is a normalized Gaussian centered at $x = \Delta_{pp}$ that describes the intensity profile of the probe beam, and $\eta(x,t)$ is the carrier distribution created by the pump pulse. At $t = 0$ this distribution will mirror the intensity profile of the pump beam and spread with increasing time. It can be written as:

$$\eta(x, t) = \int_{-\infty}^{\infty} I(x')p(x - x', t)\mathrm{d}x' \quad (2)$$

where $I(x)$ is the optical intensity profile of the focused pump laser beam used in the experiment (represented by a normalized Gaussian) and $p(\xi,t)$ describes the diffusional spreading of N carriers from an initial point located at $\xi = 0$, i.e.:

$$p(\xi, t) = \frac{N}{\sqrt{4\pi Dt}}\exp\left(-\frac{t}{\tau}\right)\exp\left(-\frac{\xi^2}{4Dt}\right) \quad (3)$$

dx.doi.org/10.1021/nl400265b | Nano Lett. 2013, 13, 1336–1340

In this expression τ is the free carrier lifetime and D is the ambipolar diffusion constant.[28]

Figure 5 compares this diffusional model (eq 1) with the experimentally observed SSPP transient signals from NW2. The experimental data shows a steady increase in the spreading of the carrier cloud, reaching several micrometers in a few hundred picoseconds. The calculated curves (Figure 5B) were obtained using the ambipolar diffusion constant for bulk Si ($D \sim 18$ cm^2/s) and a carrier lifetime $\tau = 380$ ps. The calculated curves qualitatively resemble those observed in the SSPP experiment, indicating that diffusional processes in Si nanowires grown by a VLS mechanism are remarkably similar to those in single-crystalline bulk Si materials. There are differences, however, particularly at smaller pump−probe displacements and shorter time delays. In this regime, the model predicts a greater extent of diffusion than observed experimentally, a difference which could be the result of changes in the diffusion constant because of carrier scattering within the nanowires. The exact reasons are currently under investigation.

We have developed a pump−probe microscope capable of photoexciting a single nanostructure in one location and probing it in another. Experiments performed on Si nanowires enable a direct visualization of the charge cloud produced by photoexcitation of a localized spot and spreading of this cloud along the nanowire axis. The time-resolved images show clear evidence of rapid diffusion and recombination of the free carriers followed by trap carrier migration on slower time scales.

AUTHOR INFORMATION

Corresponding Author

*E-mail: john_papanikolas@unc.edu, jfcahoon@unc.edu.

Author Contributions

M.M.G. and J.R.K. contributed equally.

Notes

The authors declare no competing financial interest.

ACKNOWLEDGMENTS

This work was supported by a grant from the National Science Foundation (CHE-1213379). J.D.C., C.W.P., and J.F.C. acknowledge support from UNC-Chapel Hill start-up funding.

REFERENCES

(1) Kempa, T. J.; Cahoon, J. F.; Kim, S. K.; Day, R. W.; Bell, D. C.; Park, H. G.; Lieber, C. M. *Proc. Natl. Acad. Sci.* **2012**, *109*, 1407.

(2) Kim, S. K.; Day, R. W.; Cahoon, J. F.; Kempa, T. J.; Song, K. D.; Park, H. G.; Lieber, C. M. *Nano Lett.* **2012**, *12*, 4971.

(3) Christesen, J. D.; Zhang, X.; Pinion, C. W.; Celano, T. A.; Flynn, C. J.; Cahoon, J. F. *Nano Lett.* **2012**, *12*, 6024.

(4) Kelzenberg, M. D.; Turner-Evans, D. B.; Putnam, M. C.; Boettcher, S. W.; Briggs, R. M.; Baek, J. Y.; Lewis, N. S.; Atwater, H. A. *Energy Environ. Sci.* **2011**, *4*, 866.

(5) Mehl, B. P.; Kirschbrown, J. R.; Gabriel, M. M.; House, R. L.; Papanikolas, J. M. *J. Phys. Chem. B* **2013**, DOI: 10.1021/jp307089h.

(6) Mehl, B. P.; Kirschbrown, J. R.; House, R. L.; Papanikolas, J. M. *J. Phys. Chem. Lett.* **2011**, *2*, 1777.

(7) House, R. L.; Mehl, B. P.; Kirschbrown, J. R.; Barnes, S. C.; Papanikolas, J. M. *J. Phys. Chem. C* **2011**, *115*, 10806.

(8) House, R. L.; Kirschbrown, J. R.; Mehl, B. P.; Gabriel, M. M.; Puccio, J. A.; Parker, J. K.; Papanikolas, J. M. *J. Phys. Chem. C* **2011**, *115*, 21436.

(9) House, R. L.; Mehl, B. P.; Zhang, C.; Kirschbrown, J. R.; Barnes, S. C.; Papanikolas, J. M. *Proc. SPIE* **2009**, *7396*, 73960G.

(10) Gundlach, L.; Piotrowiak, P. *Opt. Lett.* **2008**, *33*, 992.

(11) Djurisic, A. B.; Kwok, W. M.; Leung, Y. H.; Phillips, D. L.; Chan, W. K. *J. Phys. Chem. B* **2005**, *109*, 19228.

(12) Song, J. K.; Willer, U.; Szarko, J. M.; Leone, S. R.; Li, S.; Zhao, Y. *J. Phys. Chem. C* **2008**, *112*, 1679.

(13) Johnson, J. C.; Knutsen, K. P.; Yan, H. Q.; Law, M.; Zhang, Y. F.; Yang, P. D.; Saykally, R. J. *Nano Lett.* **2004**, *4*, 197.

(14) Huang, L. B.; Hartland, G. V.; Chu, L. Q.; Luxmi; Feenstra, R. M.; Lian, C. X.; Tahy, K.; Xing, H. L. *Nano Lett.* **2010**, *10*, 1308.

(15) Carey, C. R.; Yu, Y. H.; Kuno, M.; Hartland, G. V. *J. Phys. Chem. C* **2009**, *113*, 19077.

(16) Fujino, T.; Fujima, T.; Tahara, T. *J. Phys. Chem. B* **2005**, *109*, 15327.

(17) Fu, D.; Ye, T.; Matthews, T. E.; Grichnik, J.; Hong, L.; Simon, J. D.; Warren, W. S. *J. Biomed. Opt.* **2008**, *13*, 054036.

(18) Polli, D.; Grancini, G.; Clark, J.; Celebrano, M.; Virgili, T.; Cerullo, G.; Lanzani, G. *Adv. Mater.* **2010**, *22*, 3048.

(19) Seo, M. A.; Yoo, J.; Dayeh, S. A.; Picraux, S. T.; Taylor, A. J.; Prasankumar, R. P. *Nano Lett.* **2012**, *12*, 6334.

(20) Seo, M. A.; Dayeh, S. A.; Upadhya, P. C.; Martinez, J. A.; Swartzentruber, B. S.; Picraux, S. T.; Taylor, A. J.; Prasankumar, R. P. *Appl. Phys. Lett.* **2012**, *100*, 071104.

(21) Ruzicka, B. A.; Zhao, H. *J. Opt. Soc. Am. B* **2012**, *29*, A43.

(22) Kumar, N.; Ruzicka, B. A.; Butch, N. P.; Syers, P.; Kirshenbaum, K.; Paglione, J.; Zhao, H. *Phys. Rev. B* **2011**, *83*, 235306.

(23) Schmidt, V.; Wittemann, J. V.; Gosele, U. *Chem. Rev.* **2010**, *110*, 361.

(24) Kar, A.; Upadhya, P. C.; Dayeh, S. A.; Picraux, S. T.; Taylor, A. J.; Prasankumar, R. P. *IEEE J. Sel. Top. Quant.* **2011**, *17*, 889.

(25) The n-Si wire transient depicted in Figure 2 has been inverted (i.e., multiplied by −1). The reason this wire shows an initial absorption rather than a bleach is not entirely clear; however, in other experiments on ZnO we observed (ref 5) similar sign-changes that stemmed from a Kerr lensing contribution (in addition to absorptive features) to the overall signal. This contribution could either be positive or negative, depending upon the details of the pump−probe overlap. This process could be at play in this wire.

(26) Mohite, A. D.; Perea, D. E.; Singh, S.; Dayeh, S. A.; Campbell, I. H.; Picraux, S. T.; Htoon, H. *Nano Lett.* **2012**, *12*, 1965.

(27) Allen, J. E.; Hemesath, E. R.; Perea, D. E.; Lensch-Falk, J. L.; Li, Z. Y.; Yin, F.; Gass, M. H.; Wang, P.; Bleloch, A. L.; Palmer, R. E.; Lauhon, L. J. *Nat. Nanotechnol.* **2008**, *3*, 168.

(28) Sze, S. M.; Ng, K. K. In *Physics of Semiconductor Devices*; 3rd ed.; Wiley-Interscience: New York, 2007; p 566.